JOURNAL OF SPACECRAFT AND ROCKETS
Vol. 40, No. 6, November–December 2003
This paper reprinted from AIAA Journal, Vol. 9, No. 10, 1971, pp. 2004–2013

Stress, Buckling, and Vibration of Prismatic Shells

DAVID BUSHNELL*
Lockheed Missiles & Space Company, Palo Alto, Calif.

A computer code for the general treatment of complex shells of revolution is applied to the analysis of prismatic shells such as oval cylinders, corrugated sheets, and longitudinally stiffened cylinders with stringer discreteness retained in the model. Cylinders of circular and noncircular cross section are treated as portions of very slender toroids. Corrugated and beaded panels are treated as portions of cylinders with very large radii. Longitudinally stiffened cylinders are treated as portions of very slender toroids with discrete ring stiffeners. The technique also permits analysis of buckling of cylinders with nonsymmetric pressure or thermal loading. The analysis is based on the finite-difference method which is used in conjunction with energy minimization. Several numerical examples are given. Included are convergence studies proving the validity of the technique and buckling calculations for nonuniformly loaded cylinders, externally pressurized and axially compressed elliptic cylinders, and axially compressed corrugated and beaded panels. Vibration modes and frequencies are calculated for an eccentrically stiffened cylinder in which the stringers are treated as discrete.

Nomenclature

a = radius of cylinder
A = length of semimajor axis of elliptic cylinder
B = length of semiminor axis of elliptic cylinder
b = large radius of torus
E = Young's modulus
ΔL = length of pressure band on cylinder
L = length of prismatic shell
N,M = stress resultant, moment resultant
n = circumferential wave number
p = external pressure
s = arc length
t = wall thickness
u = meridional displacement
v = circumferential displacement
w = normal displacement
χ_o = prebuckling rotation
θ = circumferential coordinate
ν = Poisson's ratio

Introduction

THE motivation behind much of the research activity in shell analysis is to reduce computer time and core storage required to solve complex problems. It is advantageous whenever possible to reduce the number of degrees of freedom required by separation of variables and to optimize computer efficiency by setting up stiffness matrices with as narrow bands as possible. Currently, problems in complex shell analysis can be classified into two groups: that which involves two-dimensional discretization and that which involves one-dimensional discretization. The two-dimensional numerical analysis generally requires one to several orders of magnitude more computer time to solve than does the one-dimensional problem. The computer time increases quadratically with the bandwidth of the stiffness matrix and linearly with the number of degrees of freedom. Matrix bandwidths for two-dimensional problems are much wider than those for one-dimensional problems and the number of degrees of freedom required for convergence to a given accuracy is greater.

Presented as Paper 71-112 at the AIAA 9th Aerospace Sciences Meeting, New York, January 25–27, 1971; submitted February 1971; revision received June 28, 1971. This work was sponsored by the Lockheed Independent Research Program.

Index categories: Structural Static Analysis; Structural Stability Analysis; and Structural Dynamic Analysis.

* Staff Scientist. Associate Fellow AIAA.

This research was motivated by the need for economical computer solutions to problems traditionally associated with two-dimensional numerical analyses but amenable by means of an exchange of independent variables to solution by separation of variables with consequent reduction to one-dimensional numerical treatment. In this class are included stress, buckling and vibration problems for simply-supported prismatic shells. Stress analysis can be performed for prismatic shells with loads that vary in the two coordinate directions. Buckling and vibration analyses are restricted to systems in which both the loads and the geometry are prismatic-constant in the axial direction.

Figure 1 gives examples of prismatic shells: 1a is an oval cylinder which may be subjected to combinations of pressure and axial loading; 1b is a cylinder with a pressure or thermal load which varies in the circumferential direction; 1c and 1d represent typical advanced structural panels being considered for hypersonic cruise vehicles, lightweight space systems shrouds, and space shuttles; and 1e shows a general prismatic shell with stringers which can be treated as discrete elastic structures. The oval cylinder under axial compression has been investigated by Kempner and Chen,[1] Hutchinson,[2] and Almroth, Brogan, and Marlowe.[3] Elliptic cylinders under external pressure have been treated by Yao and Jenkins.[4] Liaw[5] gives a survey of papers published before April 1969 on the stability of cylindrical and conical shells of noncircular cross section. Buckling allowables for nonuniformly loaded cylinders have been calculated by Almroth[6] who investigated band-loaded cylinders in which the external pressure varies as $p_o + p_1 \cos\theta$ in the circumferential direction. Ross[7] determined experimentally critical temperatures of cylinders heated along an axial strip. Local buckling and crippling loads for axially compressed corrugated and beaded sheets have been determined theoretically and experimentally by Plank, Sakata, Davis, and Richie.[8] Buckling loads were determined experimentally by Shang, Marulic, and Sturm[9] for axially compressed longitudinally stiffened cylinders. The geometry of the specimens of Ref. 9 was such that the circumferential buckling half wave-length and stringer spacing were approximately equal, indicating the need for analytical treatment of the stringers as discrete. Egle and Sewall[10] and McDonald[11] have calculated vibration frequencies for cylinders with stringers included as discrete structures.

The structures shown in Fig. 1 and analyzed in Refs. 1–11 are all prismatic. If they are simply supported at the generator ends they can be analyzed as portions of shells of revolu-

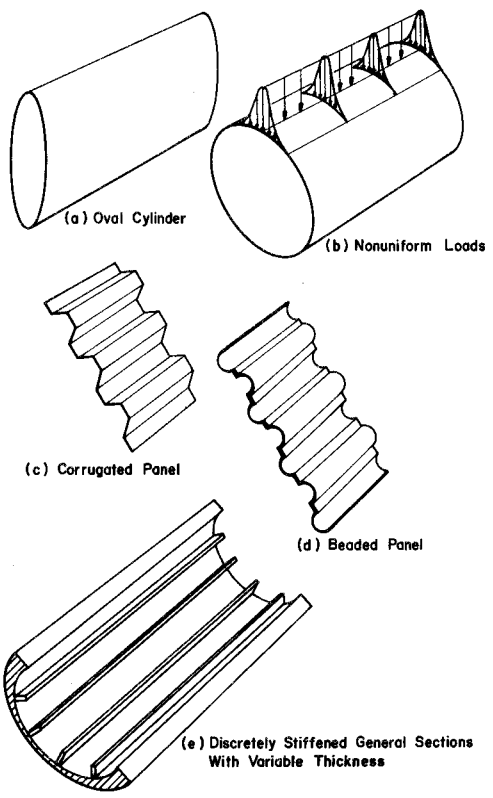

Fig. 1 Some typical prismatic shell structures.

tion in which the length of the prismatic shell is given by

$$L = \pi b/n \tag{1}$$

where b is the radius from an axis of revolution to some reference surface and n is the number of complete circumferential waves. The results presented here were thus obtained by means of the analysis and computer program described in Refs. 12–14.

Analysis

Buckling of oval cylinders or nonsymmetrically loaded cylinders can be treated by a modeling of the cylinder as a portion of a torus with a very large radius b. Figure 2 illustrates the model. A cylinder of length L, small diameter d and thickness t is modeled as a small portion of a torus with radius b. As $b \rightarrow \infty$ and L = constant the short curved cylinder approaches a straight cylinder. The cross section need not be circular, nor the thickness constant. The pressure can vary along the length as well as over the circumference. A limitation of the model is that the cylinder must be simply-supported at the ends $\theta \cdot b = 0$ and $\theta \cdot b = L$.

Since the torus is a shell of revolution, the BOSOR3 code[14] can be used to analyze it without any special alteration. What has been done here in effect is to exchange the independent variables in the analysis of a cylinder: the axial variable s for the cylinder becomes the circumferential variable $\theta \cdot b$ for the torus and visa versa. The circumferential displacement distribution of the cylinder, conventionally expressed in terms of $\sin n\theta$ or $\cos n\theta$ with n the input circumferential wave number, becomes the meridional displacement distribution of the torus, now expressed in terms of the displacement values at discrete mesh points in the finite difference analysis. Similarly, the meridional displacement distributions of the cylinder, conventionally expressed as discrete mesh point variables are now expressed in terms of $\sin n\theta$ or $\cos n\theta$ with n the number of waves around the large-diameter torus. Given the radius b, the length of the cylinder is determined by the wave number n, which in the limit of very large

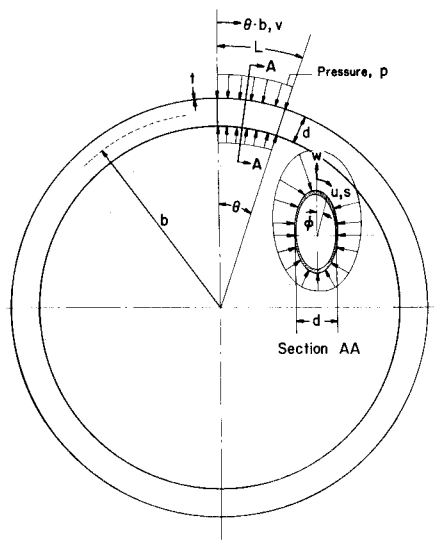

Fig. 2 Noncircular cylinder treated as portion of torus with large radius b and length $L = \theta \cdot b$.

b is a very large number (like 10,000, for example). The boundary conditions at $\theta \cdot b = 0$ and $\theta \cdot b = L$ are simple support: $N_\theta = M_\theta = u = w = 0$. The user has no choice of boundary conditions at $\theta \cdot b = 0$ and $\theta \cdot b = L$, since the simple-support condition arises from the underlying assumption that the dependent variables and their derivatives vary in this direction as $\sin n\theta$ and $\cos n\theta$.

The loading on the cylinder in Fig. 2 is expressed as a Fourier expansion over the interval $-L \leq \theta \cdot b \leq L$. For example, the pressure loading in Fig. 2 (uniform for $0 \leq \theta \cdot b \leq L$ and variable around the circumference, s) is expressed as a Fourier sine series, thus:

$$p(s,\theta) = f(s) \cdot g(\theta) \tag{2}$$

in which

$$g(\theta) = \frac{4}{\pi} \sum_{m=1,3,5\ldots}^{\text{NMAX}} \sin(m\pi\theta \cdot b)/L \tag{3}$$

The integer m is the number of half-waves in the interval $0 \leq \theta \cdot b \leq L$. Therefore, the corresponding wave number n for the complete torus is $n = m\pi b/L$. The question arises, why

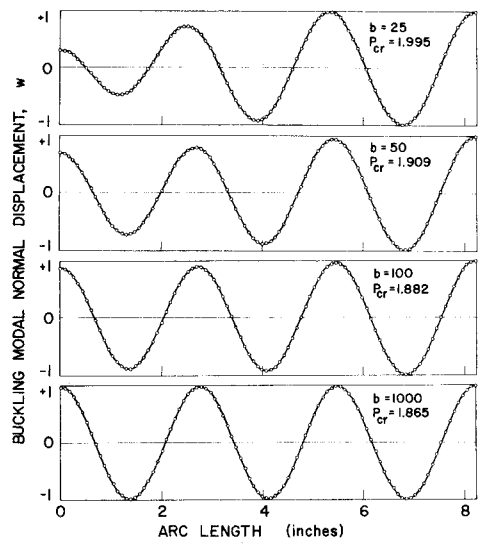

Fig. 3 Analysis of simply supported circular cylinder as portion of torus with radius b. Convergence study with increasing b. $P_{cr} = p_{cr}a/Et$, $L/a = 0.6$, $a/t = 100$, $a = 5.236$ in. One quarter of circumference covered.

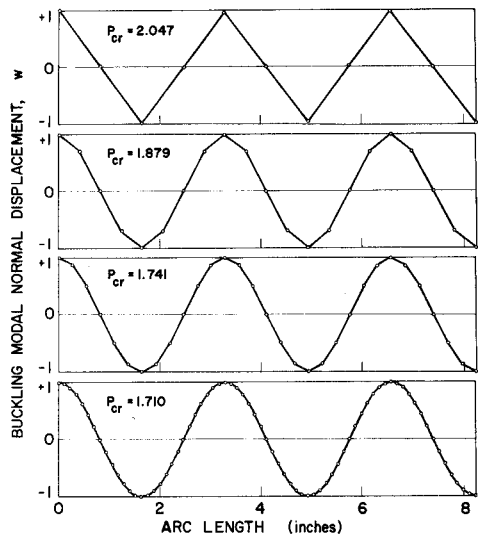

Fig. 4 Analysis of circular cylinder as torus. Mesh point convergence study.

not expand the load in a cosine series in the interval $-L \leq \theta \cdot b \leq L$? This is not possible because the $m = 0$ term corresponds to an infinite cylinder ($L = 2\pi b$). The longest half wavelength in the Fourier expansion of the load must be equal to L or an integer fraction of L.

Thus, the finite-length, simply-supported, oval cylinder under external pressure is analyzed as a toroidal shell with very large radius b and submitted to loads which vary rapidly around the circumference. In the section "Numerical Results" the behavior of a simply-supported externally pressurized elliptical cylinder is discussed.

There are additional advantages of being able to analyze cylinders in this manner. Note in Fig. 1 that the wall properties (thickness, modulus) in the s-direction need not be constant. Also, note that longitudinal stringers can be included in the analysis as discrete elastic structures. With the cylinder analyzed as a portion of a torus, the cylinder stringers are rings in this application of the BOSOR3 code. Also, cylindrical or flat panels with corrugations, beads, or other geometrical peculiarities and with arbitrary boundary conditions along generators can be treated, since the generators are now meridional stations. Some of these cases are discussed in the following sections.

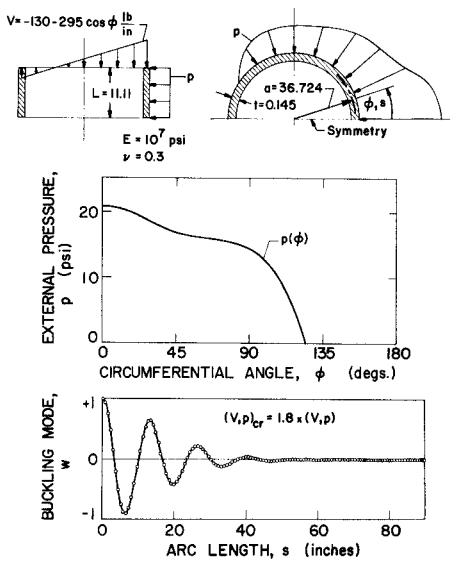

Fig. 5 Buckling mode of nonuniformly loaded, simply supported circular cylinder. Critical load = 1.8 times the load distribution shown.

Table 1 Convergence of critical lateral pressure parameter[a] $P_{cr} = p_{cr}a/Et$

b, in.	$L/a = 0.6$, $a = 5.236$ in. $P_{cr}^{(10)b}$	$P_{cr}^{(12)b}$	$L/a = 6.0$, $a = 0.5236$ in. $P_{cr}^{(4)b}$	$P_{cr}^{(6)b}$
10			0.26141	0.38559
25	1.8467	1.9949	0.19387	0.33774
50	1.7790	1.9090	0.17486	0.33036
100	1.7415	1.8815	0.16668	0.32789
500	1.7129	1.8664	0.16085	0.32648
1,000	1.7095	1.8649	0.16017	0.32634
5,000	1.7068	1.8638	0.15964	0.32623
10,000	1.7065	1.8637	0.15957	0.32620
∞	1.7024 ← (Flügge)		0.15943 ← (Flügge)	

[a] With increasing toroidal radius b for shells with $a/t = 100$, $E = 10^6$ psi, $\nu = 0.3$.
[b] Superscripts in parentheses represent the total number of waves around the circumference of the cylinder.

Convergence Studies

The application of BOSOR3 to the stability analysis of cylinders of noncircular cross section and nonsymmetrical loads was validated by convergence studies for uniformly loaded circular cylinders analyzed as portions of toroidal shells with various radii b and various numbers of meridional mesh points. Membrane prebuckling analysis was used in the convergence studies. For given values of b, the cylinder lengths were established as described above by selection of appropriate circumferential wave numbers, n. This procedure is valid for simply-supported cylinders the buckling modes of which have an integral number of half-sine waves along the length.

Tables 1–3 and Figs. 3 and 4 give the results for hydrostatically compressed circular cylinders. In Table 1 convergence with increasing toroidal radius b is given for cylinders with $L/a = 0.6$ and $L/a = 6.0$. The values of pa/Et for b = infinity are calculated from Eqs. (11) and (12), pp. 424–425 of Flügge.[15] The lowest two eigenvalues are obtained in each case. In the limit of very large b these eigenvalues correspond to two wave numbers, $n = 10$ and $n = 12$. Figure 3 shows the normalized buckling displacement w for the second eigenvalue for increasing values of toroidal radius b. With large b the distribution over $\frac{1}{4}$ of the circumference of the cylinder approaches a cosine wave with three full waves. This mode corresponds to $n = 12$ for the complete cylinder. Symmetry conditions are imposed at the ends of the toroidal meridian. All calculations were performed in double precision on the Univac 1108. The data points in Fig. 3 indicate finite difference mesh points.

Table 2 and Fig. 4 represent the results of a convergence study in which the number of mesh points is varied for a

Table 2 Mesh point convergence study for simply-supported circular cylinder[a]

Number of mesh points per half-wave	$L/a = 0.6$, $a = 5.236$ in. $P_{cr}^{(10)}$	$L/a = 6.0$, $a = 0.5236$ in. $P_{cr}^{(4)}$
2	2.0467	0.21976
4	1.7886	0.17209
6	1.7409	0.16491
8	1.7242	0.16250
10	1.7164	0.16141
14	1.7097	0.16046
19	1.7065	0.16002
25	...	0.15979
35	...	0.15964
48	...	0.15957
∞	1.7024	0.15943

[a] Analyzed as portion of torus with radius $b = 10{,}000$, $a/t = 100$, $E = 10^6$ psi, $\nu = 0.3$. Critical lateral pressure parameter $P_{cr} = p_{cr}a/Et$.

Table 3 Mesh point convergence study for simply-supported circular cylinder analyzed as a cylinder[a]

Number of axial mesh points	Critical lateral pressure, P_{cr}
5	1.7146
10	1.7063
20	1.7035
30	1.7029
50	1.7025
80	1.7024
97	1.7024

[a] $P_{cr} = p_{cr}a/Et$, $a/t = 100$, $E = 10^6$ psi, $\nu = 0.3$, $L/a = 0.6$, $a = 5.236$ in.

given (very large) value of b. The buckling modes plotted in Fig. 4 correspond to $n = 10$ waves around the circumference of the cylinder with $L/a = 0.6$. Table 3 gives the convergence of buckling loads with increasing mesh points for the cylinder with $L/a = 0.6$ analyzed as a cylinder, not as a portion of a large-radius torus. These convergence studies indicate the degree of accuracy obtained with the BOSOR3 code and provide a guide to the user of STAGS[3] or other large-scale two-dimensional computer codes as to the number of mesh points required for adequate accuracy.

Numerical Results

In this section numerical results are presented for nonuniformly loaded circular cylinders, externally pressurized and axially compressed noncircular cylinders, axially compressed corrugated and beaded panels and circular cylinders with stringers treated as discrete elastic structures.

Nonuniformly Loaded Cylinders

Figure 5 shows a short cylinder submitted to axial compression and external pressure which vary around the circumference. The cylinder is simply-supported at both ends. Pressure and axial load vary as shown in the figure. In the stability analysis the peak axial load and pressure have a constant ratio, so that the eigenvalue λ represents a factor to be multiplied by the load distributions given in Fig. 5. The short cylinder is analyzed as a toroidal segment with radius $b = 35{,}369$ and $n = 10{,}000$ circumferential waves. Membrane prebuckling theory is used. An eigenvalue $\lambda = 1.8$ is found from BOSOR3. The buckling modal displacement

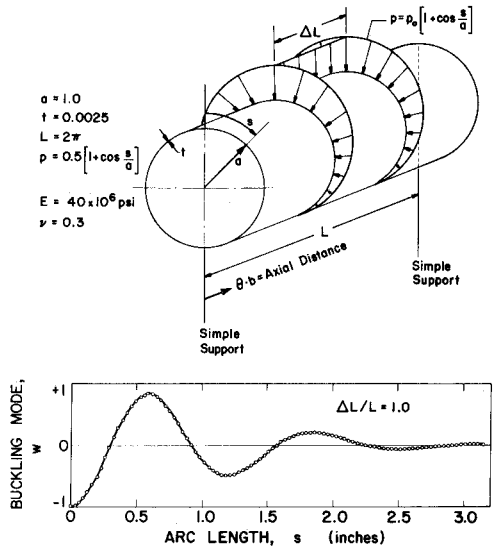

Fig. 6 Buckling mode for nonsymmetrically loaded cylinder with $p_{cr}a/Et \times 10^5 = 2.292$, $\Delta L/L = 1.0$.

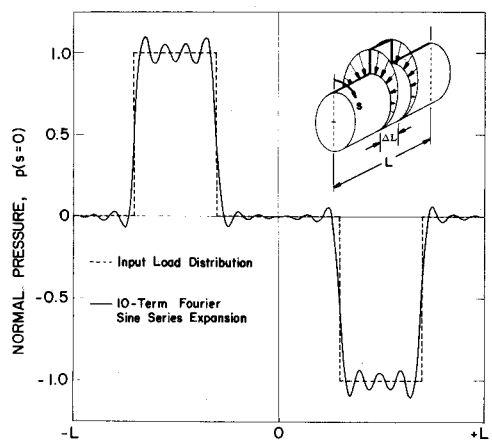

Fig. 7 Pressure distribution on cylinder for $\Delta L/L = 0.4$. Cylinder modeled in BOSOR3 as portion of torus (see Fig. 2).

is also shown in Fig. 5. Symmetry conditions were imposed at $s/a = 0°$ and $s/a = 180°$.

An analysis was made of a simply-supported cylinder submitted to a band pressure load which varies around the circumference as shown in Fig. 6. The cylinder was analyzed as a portion of a torus with $b = 20{,}000$ in. and $n = 10{,}000$. Comparisons were made with the theory of Almroth[6] for a cylinder with $a = 1.0$ in., $t = 0.0025$ in., $L = 2\pi$ in. and $\Delta L/L = 1.0$ and 0.4. For the case $\Delta L/L = 1.0$, Almroth obtains $p_{CR}a/(Et) \times 10^5 = 2.253$. The BOSOR3 program yields a value 2.292 for this parameter. The buckling modal displacement w is shown at the bottom of Fig. 6.

Figure 7 shows the normal pressure loading at $s = 0$ on the cylinder with $L = 2\pi$, $a/t = 400$ and $\Delta L/L = 0.4$. The load is expanded in a 10-term Fourier sine series in the interval $-L \leq \theta \cdot b \leq +L$ (see Fig. 2). Figure 8 gives the axial distributions of stress resultants corresponding to the 10-term Fourier sine series expansion of the banded pressure load shown in Fig. 7. Figure 9 shows the circumferential distribution of stress resultants at the cylinder midlength $\theta \cdot b = \pi$. These values are used in the stability analysis, in which the assumption is made that they are constant around the circumference of the equivalent torus (along the axis of the cylinder). Therefore, the buckling loads calculated in BOSOR3 are independent of the bandwidth of the pressure for bandwidths that are long compared to a boundary layer length, $(at)^{1/2}$. Thus, $p_{CR}a/(Et) \times 10^5 = 2.292$ compared to the value of 3.0913 obtained with Almroth's more exact analysis.[6]

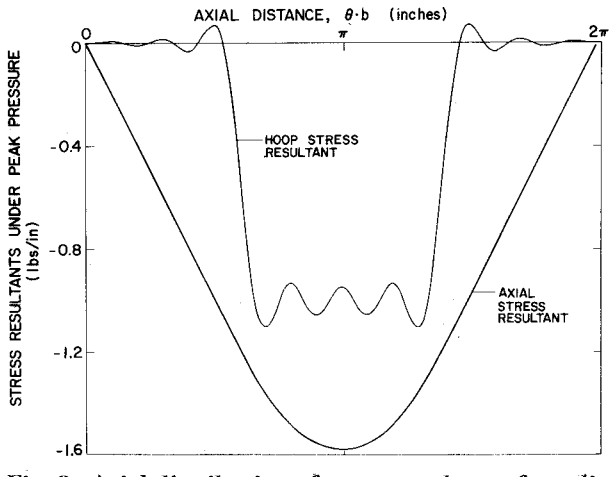

Fig. 8 Axial distribution of stress resultants for cylinder under band pressure load ($\Delta L/L = 0.4$).

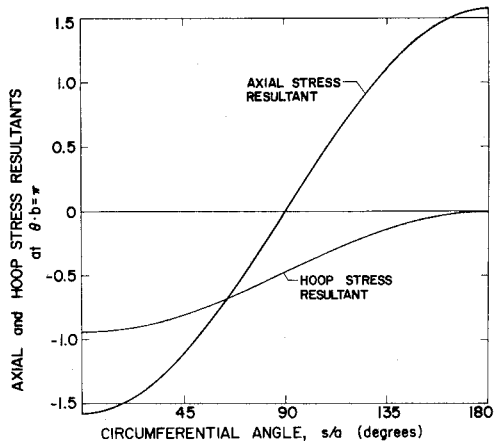

Fig. 9 Circumferential distributions of stress resultants at cylinder midlength $\theta \cdot b = \pi$.

Stress and Buckling of Elliptic Cylinders

Figure 10 shows an elliptic cylinder and gives various dimensions and material properties. The cylinders are submitted to uniform external pressure on the curved surface only. Yao and Jenkins[4] obtained buckling pressures from tests on simply-supported polyvinyl chloride shells. They compared the test results with a theory in which the prebuckled state is calculated from linear membrane theory. Buckling pressures are obtained from an eigenvalue problem based on the Galerkin method. Prebuckling rotations are neglected in the theory of Ref. 4.

The BOSOR3 computer program was used to calculate stresses and buckling pressures for elliptic cylinders of the geometries shown in Fig. 10. The oval cylinders were analyzed as toroidal shells with very large b and n as described above. The uniform external pressure was expanded in a 20-term Fourier sine series according to Eqs. (2) and (3). Figure 11 shows the axial distributions of normal displacement and in-plane stress resultants at $s = 0$ (end of minor axis B) for an external pressure of 1 psi on an elliptic cylinder with $A/B = 2$, $t = 0.019$, and various values of L. The quantity $\theta \cdot b/L$ is the normalized distance along the circumference of the torus of radius b (see Fig. 2). Figure 12 shows the circumferential distributions at midlength of rotation about a generator and in-plane stress resultants. Plots cover $\frac{1}{4}$ of the circumference. The stress distributions are very similar to those predicted by membrane theory. Results were obtained by Fourier sine series expansion of the uniform axial pressure distribution [see Eq. (3)] with twenty terms included in the series. Three hundred degrees of freedom were used, and 1 min, 56 sec of UNIVAC 1108 time were required for the double-precision calculations. The prestress state was checked by a run with the linear version of the two-dimensional finite-difference program, STAGS.[3] Excellent agreement was obtained.

Note that as the length L of the shell increases the hoop stress resultant at $L/2$ seems to approach the membrane value

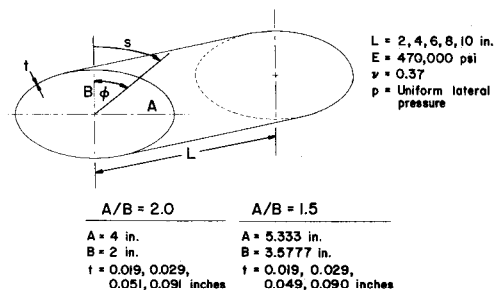

Fig. 10 Simply supported elliptic cylinder configurations.

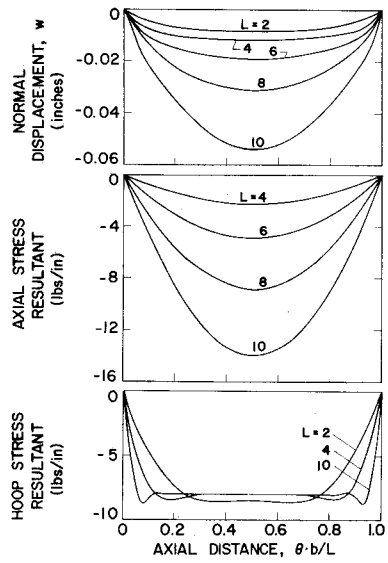

Fig. 11 Displacement w and stress resultants at $s = 0$ for 1 psi; external pressure on elliptic cylinder with $A/B = 2$, $t = 0.019$.

$pa = -8.0$ lb/in. at the end of the minor axis ($s = 0$) and $pa = -1.0$ lb/in. at the end of the major axis. However, from simple static equilibrium conditions it is known that as $L \to \infty$ the hoop stress resultant approaches -2 lb/in. at $s = 0$ and -4 lb/in. at $s = s_{end}$ for uniform external pressure of 1 psi. Clearly, the elliptical cylinders of length 4–10 in. with cross sections as shown in Fig. 10, while long compared to bending boundary-layer lengths, are short compared to lengths required for the effect of end cross section fixity to die out.

Buckling pressures were calculated for several cases with $A/B = 2.0$ and $A/B = 1.5$. The results, compared with Yao and Jenkins[4] tests and theory, are presented in Figs. 13–17 and Tables 4–6. Predicted buckling pressures are always higher than the test values and are rather inaccurate for the thicker shells. The thicker shells apparently buckle by collapsing gradually rather than failing by a sudden change (bifurcation) in the mode of deformation (see Fig. 4 of Ref. 4). It is probable, therefore, that the present theory is not valid for the shells with nominal thickness 0.050 and 0.090 in.

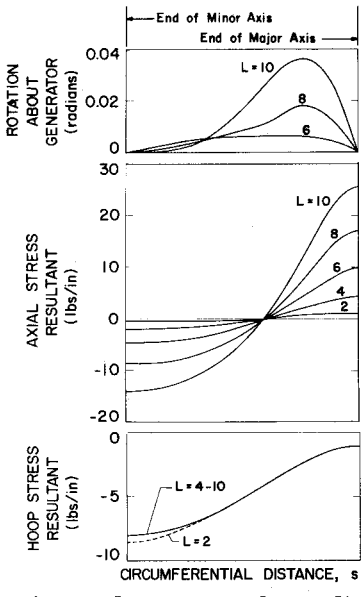

Fig. 12 Rotation and stress resultant distributions at midlength of elliptic cylinder with $A/B = 2$, $t = 0.019$.

Table 4 Buckling pressures of elliptical cylinders with $A/B = 2$ and various lengths and thicknesses[a]

		Buckling pressures, psi				
		Theory			Test	Test/ BOSOR3
Thickness t, in.	Length L, in.	BOSOR3 p_{cr}^1	BOSOR3 with $\chi_o = 0$ p_{cr}^2	Yao and Jenkins p_{cr}^3	Yao and Jenkins p_{cr}^T	p_{cr}^T/p_{cr}^1
0.019	2	0.730	0.797	0.714	0.613	0.84
	4	0.368	0.381	0.331	0.324	0.88
	6	0.246	0.259	0.217	0.239	0.97
	8	0.189	0.203	0.166	0.189	1.00
	10	0.150	0.170	0.133	0.140	0.93
0.029	2	2.16	2.47	2.23	1.88	0.87
	4	1.11	1.16	1.00	0.877	0.79
	6	0.739	0.788	0.661	0.665	0.90
	8	0.567	0.621	0.499	0.533	0.94
	10	0.437	0.502	0.390	0.411	0.94
0.051	2	10.0	11.5	10.12	...	...
	4	4.71	5.13	4.33	3.10	0.66
	6	3.20	3.53	2.82	2.21	0.69
	8	2.26	2.64	2.03	1.54	0.68
	10	1.63	2.15	1.63	1.14	0.70
0.091	2	57.2	57.6	50.5	...	...
	4	20.5	24.4	20.1	...	...
	6	13.4	15.9	12.5	7.77	0.58
	8	9.23	12.2	9.42	5.81	0.63
	10	5.87	10.6	8.23	4.46	0.76

[a] $E = 470{,}000$ psi, $\nu = 0.37$, $A = 4.0$ in., $B = 2.0$ in.

A nonlinear, two-dimensional collapse analysis such as that of Ref. 3 is required for these cases. This analysis has been performed by Marlowe and is reported in Ref. 16.

Figures 15–17 show the buckling modes for externally pressurized elliptical cylinders with $A/B = 2$, lengths $L = 2, 4, 6, 10$ in. and thickness $t = 0.019, 0.029$ and 0.091 in. Note that the plot corresponding to $L = 10$ in Fig. 15 covers $0 \leq \varphi \leq 180°$ of arc length, whereas all other plots in Figs. 15–17 cover $0 \leq \varphi \leq 90°$. With the exception of the case $A/B = 2$, $L = 10$, $t = 0.019$, the buckling loads given in Figs. 13–14 correspond to modes symmetrical about the ends of both the minor and major axes. The lowest buckling pressure for the exceptional case corresponds to displacements symmetrical about $\varphi = 0°$ and antisymmetrical about $\varphi = 90°$. For all cases modes antisymmetrical and symmetrical about $\varphi = 90°$ correspond to pressures within a few percent of each other.

Table 5 Buckling pressures of elliptical cylinders with $A/B = 1.5$ and various lengths and thicknesses[a]

		Buckling pressures, psi				
		Theory			Test	Test/ BOSOR3
Thickness t, in.	Length L, in.	BOSOR3 p_{cr}^1	BOSOR3 with $\chi_o = 0$ p_{cr}^2	Yao & Jenkins p_{cr}^3	Yao & Jenkins p_{cr}^T	p_{cr}^T/p_{cr}^1
0.019	2	0.706	0.768	0.683	0.600	0.85
	4	0.345	0.349	0.316	0.300	0.87
	6	0.228	0.231	0.207	0.214	0.94
	8	0.172	0.176	0.155	0.167	0.97
	10	0.138	0.143	0.125	0.131	0.95
0.029	2	2.08	2.36	2.15	1.60	0.77
	4	1.04	1.05	0.952	0.874	0.84
	6	0.678	0.691	0.621	0.610	0.90
	8	0.511	0.525	0.466	0.496	0.97
	10	0.408	0.424	0.371	0.403	0.99
0.049	2	8.60	9.76	9.45	...	...
	4	3.99	4.14	3.96	3.07	0.77
	6	2.64	2.71	2.54	2.22	0.84
	8	1.97	2.04	1.89	1.69	0.86
	10	1.60	1.69	1.51	1.38	0.86
0.090	2	50.7	52.7	49.7	...	...
	4	18.6	20.8	19.1	...	...
	6	12.7	13.4	12.0	9.52	0.75
	8	9.66	10.3	8.88	7.63	0.79
	10	7.51	8.21	7.01	5.86	0.78

[a] $E = 470{,}000$ psi, $\nu = 0.37$, $A = 5.3333$ in., $B = 3.5777$.

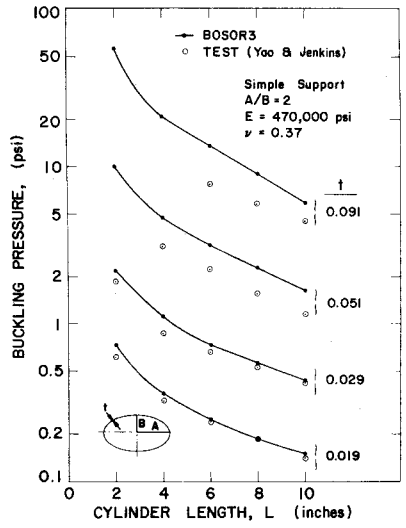

Fig. 13 Buckling loads for elliptic cylinders with $A/B = 2$.

Tables 4 and 5 give buckling pressures in psi for the simply supported elliptical cylinders with $A/B = 2$ and 1.5, respectively. Theoretical values are compared with Yao and Jenkins' test results.[4] Three theoretical values, p_{CR}^1, p_{CR}^2, and p_{CR}^3, are given for each geometry. The p_{CR}^1 corresponds to BOSOR3 results with both prebuckling in-plane stress resultants and prebuckling rotations χ_o about the generators included in the stability analysis. The p_{CR}^2 are calculated neglecting the cross section shape change (effect of χ_o) in the stability analysis. Note that the χ_o effect becomes larger as L and t increase. The p_{CR}^3 are the analytical results from Ref. 4.

Table 6 gives convergence properties of buckling pressures for the elliptical cylinders $A/B = 2$, $L = 10$ in., and various values of t. The number of terms in the Fourier sine series representation of the axial load distribution is varied. In this study the value of the pressure at the midlength of the cylinder is maintained at unity, independent of the number of terms taken in the series.

Cylinders of Noncircular Cross Section under Axial Compression

Buckling loads and post-buckling behavior have been determined for axially compressed cylinders of oval cross section by Kempner and Chen[1] and Hutchinson.[2] Almroth, Brogan and Marlowe[3] have studied the nonlinear behavior of axially compressed oval cylinders through use of a two-dimensional finite difference analysis. The BOSOR3 program can be used

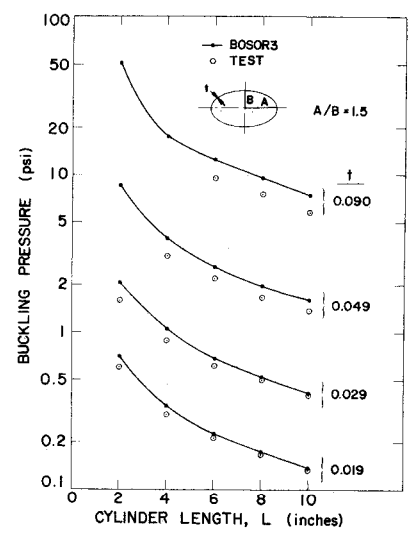

Fig. 14 Buckling loads for elliptic cylinders with $A/B = 1.5$.

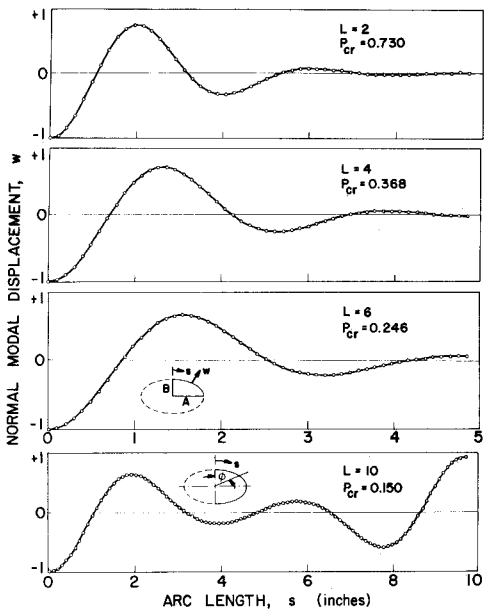

Fig. 15 Buckling modes of elliptic cylinders with $A/B = 2$, $t = 0.019$ in. and $L = 2$, 4, 6, and 10 in.

to determine bifurcation buckling loads from linear theory for axially compressed, simply supported elliptic cylinders. Membrane prebuckling theory is used in the analysis. The cylinder is treated as a portion of a large-radius torus. Figure 18 shows the buckling displacements in the circumferential direction for $0 \leq \varphi \leq 180°$. The axial distribution is a half-sine wave. The lowest two eigenvalues are very close to each other, and the modes are symmetric and antisymmetric about $\varphi = 90°$.

Figure 19 shows buckling modes for an axially compressed simply supported cylinder with a pear-shaped cross section. Membrane theory was used in the prebuckling analysis. The lowest two eigenvalues, $N_{cr} = 24.02$ lb/in. and 34.74 lb/in. correspond to uniform loading over the entire perimeter of the cross section, and the highest eigenvalue, $N_{cr} = 586$ lb/in., corresponds to loading over the curved portions only. Symmetry conditions were imposed at points A and B. The axial displacement variation is a half-sine wave. The lowest two eigenvalues correspond to the plates buckling. For axial loads higher than 35 lb/in. the plates are considered to be buckled and carrying no load. The third buckling mode in Fig. 19 therefore corresponds to a model in which only the curved portions of the pear-shaped cylinder are loaded. The buckling mode is similar to the displacement distribution corresponding to collapse obtained with the two-dimensional STAGS programs.[17] However, a much lower collapse load is obtained with STAGS, presumably because the prebuckling deformations in the flat plate segments propagate into the curved segments with increasing load, introducing imperfections into an imperfection-sensitive structure. The axial load at collapse integrated over half of the cross section perimeter is 1186 lbs according to STAGS and 1840 lb according to BOSOR3. The critical load for half of a perfect cylinder is 1880 lb.

Table 6 Convergence of elliptical cylinder buckling pressures (psi)[a]

t	1 term	3 terms	5 terms	9 terms
0.019	0.152	0.151	0.150	0.150
0.029	0.449	0.442	0.438	0.437
0.051	1.73	1.65	1.63	1.63
0.091	6.97	6.32	6.05	5.87

[a] With increasing numbers of terms in the Fourier sine series expansion of uniform pressure: $A/B = 2$, $L = 10$ in.

The reduction in predicted buckling load from 1880–1840 lbs is due to the fact that the curved portion is joined to a flat portion, rather than being a complete cylinder. The much larger reduction from 1840–1186 lb is due to the inclusion in the STAGS analysis of the prebuckling deformation which propagates from the flat portions into the curved portions, rendering imperfect these imperfection-sensitive parts of the shell. The BOSOR3 analysis is performed by treatment of the cylinder as a shell of four segments, indicated in Fig. 19. Finite difference mesh points are indicated by small circles.

Buckling of Axially Compressed Corrugated and Beaded Panels

Figures 1c and d show typical advanced structural panel designs proposed for hypersonic vehicles and the space shuttle. Reference 8 presents test and theoretical results for several panel configurations subjected to axial compression and shear at room temperature and elevated temperature. Panels were tested for general (panel) buckling and local crippling loads. In Ref. 8 buckling predictions are based on wide-column theory and simply-supported orthotropic plate theory. Local crippling predictions are based on simple buckling formulas derived for constant-thickness plate and cylindrical elements representative of individual components of the complex panels.

Two configurations are analyzed for critical axial loads in this paper: a trapezoidal corrugation and a beaded corrugation. The geometry is shown in Fig. 20. The thickness distributions and dimensions are taken from Ref. 8. The thickness of the beaded panel (Fig. 20a) is assumed in the present analysis to vary linearly between stations where it is called out. That of the trapezoidal corrugations is assumed constant in each of the flat elements. The panels are treated in BOSOR3 as segmented shells of revolution with very large radii b: for the beaded panel $b = 10^5$ in. and for the trapezoidal-corrugated panel $b = 10^4$ in. Figure 20 shows the division of the panels into segments with symmetry planes at which either antisymmetry conditions or symmetry conditions are imposed in the stability analysis.

Figure 21 shows critical axial load/length N_{CR} for the beaded panel of Fig. 20 as a function of wave number n or

Table 7 Stiffened cylinder vibration frequencies (cps)

	Cylinder analyzed as cylinder			Cylinder analyzed as portion of torus		
Circumferential wave number →	1	2	3	1	2	3
No rings or stringers	1889	778.3	627.1		777.19	625.57
No rings, stringers smeared	1758	805.8	641.2			
Rings smeared, no stringers	1695	977.2	2159	1694	976.0	
Rings and stringers smeared	1623	958.9	1903	1623	957.9	
Rings discrete, no stringers	1671	853.0	1394			
Rings discrete, stringers smeared	1611	898.5	1504			
No rings, stringers discrete					802.6	630.3
Rings smeared, stringers discrete				1618	960.7	
Rings and stringers discrete						

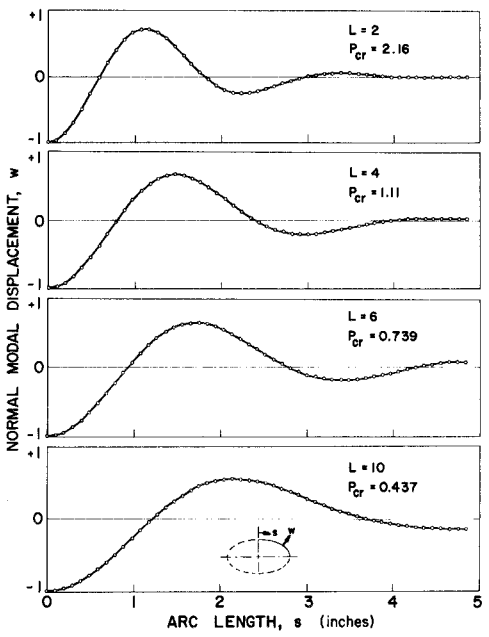

Fig. 16 Buckling modes of elliptic cylinders with $A/B = 2$, $t = 0.029$ in. and $L = 2, 4, 6$, and 10 in.

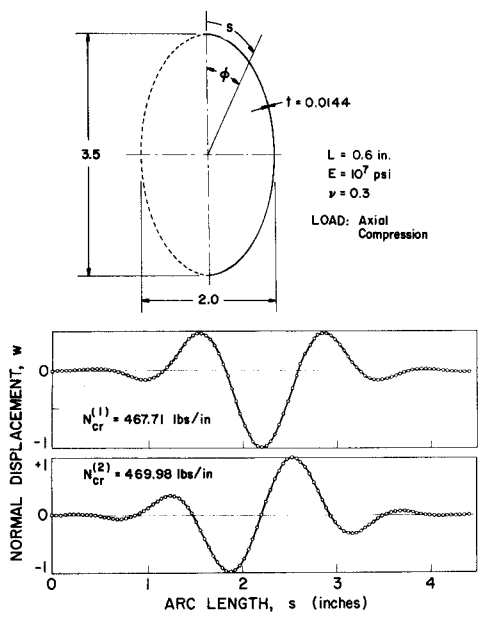

Fig. 18 Buckling modes for elliptic cylinder under axial compression.

length $L = \pi b/n$. The semilog plot covers lengths from 50–0.3 in. Three types of buckling occur in this range of L, and their corresponding mode shapes are shown in Figure 21. The lowest critical load is associated with a long-axial-wave length panel buckling from bead-crest to bead-crest. The intermediate wavelength load corresponds to buckling of the beads as axially compressed perfect cylinders, and the calculated N_{CR} from $n = 150{,}000$–$400{,}000$ is very close to the classical value $0.6Et^2/R$. The shortest length crippling load corresponds to buckling of the flat regions 0.556 in. wide between beads. The dotted curves represent critical axial loads for simply supported and clamped plates calculated from the appropriate formulas in Ref. 18. Two cases were run on BOSOR3, one with the angle $\alpha = 0$ (Fig. 20) and one with $\alpha = 12°$, which represents the test configuration. In the tests the long panel mode was first observed at a line load of about 412 lb/in. and a crippling mode involving both flats and beads was observed at 1250 lb/in.

The BOSOR3 code is conservative in the prediction of the long panel mode, probably because the 30-in.-long test panel was not in fact simply supported at the ends and because it was stable in this mode in the initial post-buckling range. The BOSOR3 code is very unconservative in the prediction of crippling because this mode of failure is sensitive to imperfections and occurs at average stresses approaching the proportional limit of the material.

Figure 20b shows the trapezoidal corrugated panel, analyzed as a shell with seven segments. This many segments were taken to permit general instability across the three flat segments labeled 3, 4, and 5. Such a mode would be analogous to the long panel mode of the beaded sheet. In the BOSOR3 analysis this mode did not appear, however. Nor was this type of buckling observed in the tests reported in Ref. 8.

Symmetry conditions imposed as shown in Fig. 20b permit the wide-column mode for long panels (low n). In this case the wide-column mode corresponds to the lowest eigenvalue for given wave number n if $n < 4000$ or $L >$ about 7.5 in. The wide-column mode corresponds to the critical load if $L >$ about 15 in. and the panel is free at the unloaded edges.

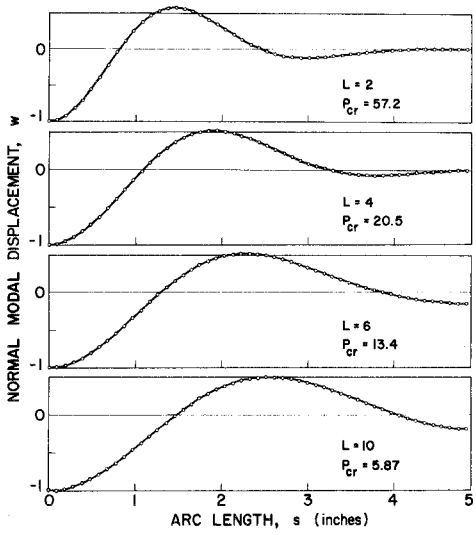

Fig. 17 Buckling modes of elliptic cylinders with $A/B = 2$, $t = 0.091$ in. and $L = 2, 4, 6$, and 10 in.

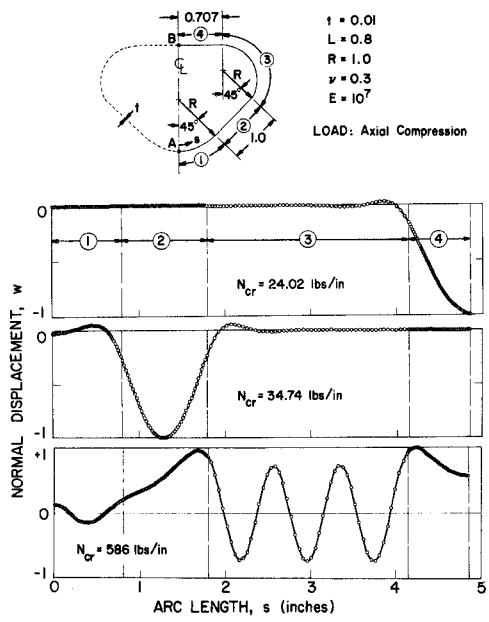

Fig. 19 Buckling modes for axially compressed pear shaped cylinder.

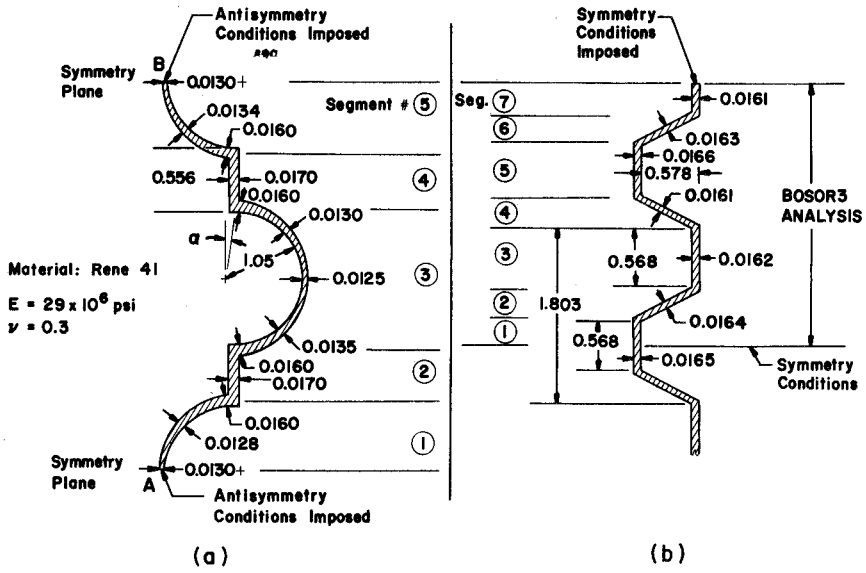

Fig. 20 Variable thickness beaded and corrugated panel configurations.

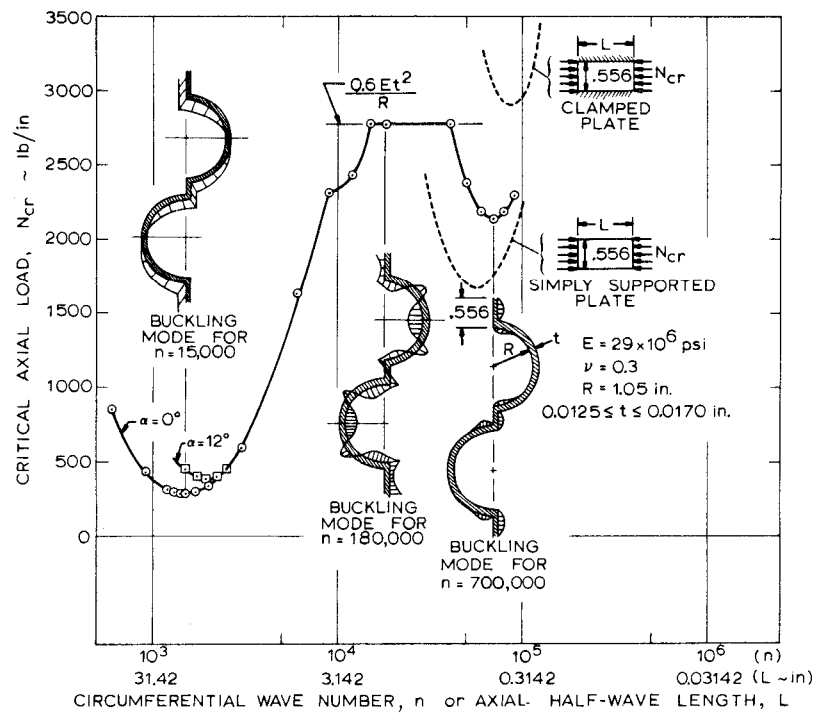

Fig. 21 Buckling loads vs length of beaded panel.

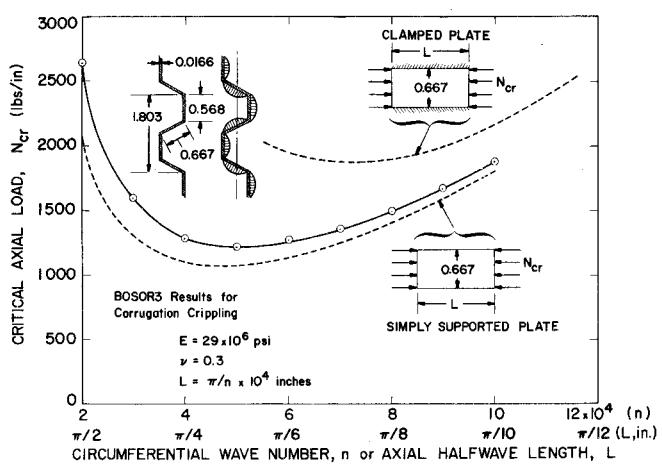

Fig. 22 Crippling loads vs length for a trapezoidal corrugated sheet.

Figure 22 shows the critical axial load versus length L or wave number n. The dotted curves represent calculations based on formulas in Ref. 18. Test values reported in Ref. 8 correspond to a line load of about 1120 lb/in. The good agreement might be expected since the critical loads for configurations consisting of flat plates are not sensitive to initial imperfections, and the average stress at failure is somewhat below the proportional limit of the material.

Vibration of Stiffened Cylinders

The stringer-stiffened shell shown in Fig. 1e is a prismatic structure. Thus, BOSOR3 can be used as described above to obtain vibration frequencies with the stringers treated as discrete, provided the shell is simply supported at the generator ends. In this section vibration frequencies are given for the ring- and stringer-stiffened circular cylinder shown in Fig. 23. The rings and stringers are considered to be attached to the shell at single points on the reference surface or to be smeared

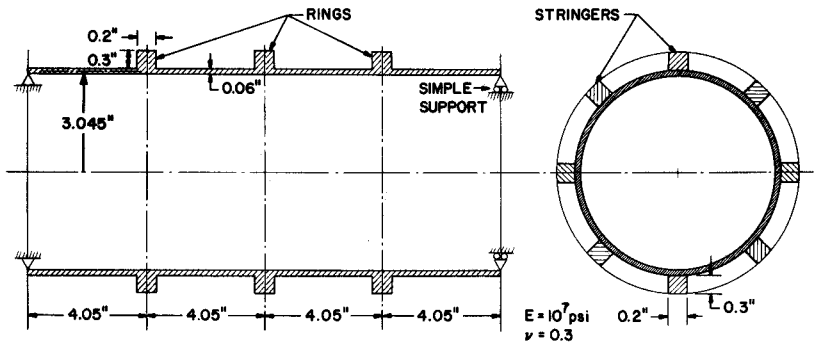

Fig. 23 Geometry of vibrating ring- and stringer-stiffened cylinder.

out in the usual way. Frequencies are calculated for several mathematical models and the results are given in Table 7. The geometry is similar to that analyzed and tested by Scruggs, Pierce, and Reese.[19] The result listed for rings discrete, no stringers for two circumferential waves agrees with that obtained by Forsberg.[20] Agreement between comparable cases run as both cylinder and torus indicates that enough mesh points were used in the analysis for adequate convergence. The results for rings smeared and no stringers, stringers smeared, and stringers discrete indicate that the stringers have little effect on the frequencies for this particular geometry. The increase in shell stiffness is countered by the increase in mass. Similar results have been found by others and are reported in Refs. 14 and 21, for example.

References

[1] Kempner, J. and Chen, Y.-N., "Postbuckling of an Axially Compressed Oval Cylindrical Shell," *Applied Mechanics Proceedings of the Twelfth International Congress of Applied Mechanics*, Stanford Univ., Aug 1968, pp. 246–256.

[2] Hutchinson, J. W., "Buckling and Initial Postbuckling Behavior of Oval Cylindrical Shells Under Axial Compression," *ASME Journal of Applied Mechanics*, Vol. 35, No. 1, March 1968, pp. 66–72.

[3] Almroth, B. O., Brogan, F. A., and Marlowe, M. B., "Collapse Analysis for Elliptic Cones," *AIAA Journal*, Vol. 9, No. 1, Jan. 1971, pp. 32–36.

[4] Yao, J. C. and Jenkins, W. C., "Buckling of Elliptic Cylinders Under Normal Pressure," *AIAA Journal*, Vol. 8, No. 1, Jan. 1970, pp. 22–27.

[5] Liaw, B. D., "A Survey of the Stability of Cylindrical and Conical Shells of Oval Cross Section," Brown Engineering Rept. RL-NXDO-610, April 1969, Brown Univ.

[6] Almroth, B. O., "Buckling of a Cylindrical Shell Subjected to Nonuniform External Pressure," *ASME Journal of Applied Mechanics*, Vol. 29, No. 4, Dec. 1962, pp. 675–682.

[7] Ross, B., Mayers, J., and Jaworski, A., "Buckling of Thin Cylindrical Shells Heated Along an Axial Strip," *Experimental Mechanics*, Vol. 5, No. 8, Aug. 1965, pp. 247–256.

[8] Plank, P. P., Sakata, I. F., Davis, G. W., and Richie, C. C., *Hypersonic Cruise Vehicle Wing Structure Evaluation*, Vol. 3, Sec. 27, Lockheed Missiles & Space Co., Sunnyvale Calif., 1970.

[9] Shang, J. C., Marulic, W. J., and Sturm, R. G., "Buckling of Longitudinally Stiffened Cylinders," *ASCE Journal of the Structural Division*, Vol. ST5, Oct. 1964, pp. 161–195.

[10] Egle, D. M. and Sewall, J. L., "An Analysis of Free Vibration of Orthogonally Stiffened Cylindrical Shells with Stiffeners Treated as Discrete Elements," *AIAA Journal*, Vol. 6, No. 3, March 1968, pp. 518–526.

[11] McDonald, D., "A Problem in the Free Vibrations of Stiffened Cylindrical Shells," *AIAA Journal*, Vol. 8, No. 2, Feb. 1970, pp. 252–258.

[12] Bushnell, D., "Analysis of Ring-Stiffened Shells of Revolution under Combined Thermal and Mechanical Loading," *AIAA Journal*, Vol. 9, No. 3, March 1971, pp. 401–410.

[13] Bushnell, D., "Analysis of Buckling and Vibration of Ring-Stiffened, Segmented Shells of Revolution," *International Journal of Solids and Structures*, Vol. 6, No. 2, Feb. 1970, pp. 157–181.

[14] Bushnell, D., "Stress, Stability, and Vibration of Complex Shells of Revolution: Analysis and User's Manual for BOSOR3," Rept. N-5J-69-1, and SAMSO TR-69-375, Sept. 1969, Lockheed Missiles & Space Co.,

[15] Flügge, W., *Stresses in Shells*, 2nd ed., Springer-Verlag, Berlin, 1962, Chap. 7, pp. 424–425.

[16] Marlowe, M. B. and Brogan, F. A., "Collapse of Elliptic Cylinders under Uniform External Pressure," AIAA Paper 71-146, New York, 1971.

[17] Bushnell, D. and Almroth, B. O., "Finite-Difference Energy Method for Nonlinear Shell Analysis," Lockheed Missiles & Space Co., Computer-Oriented Analysis of Shell Structures Conference, Palo Alto, Calif., Aug. 1970.

[18] Timoshenko, S., *Theory of Elastic Stability*, pp. 329 and 345, McGraw-Hill, New York, 1936, Chap. 7.

[19] Scruggs, R. M., Pierce, C. V., and Reese, J. R., "An Analytical and Experimental Study of the Vibration of Orthogonally Stiffened Cylindrical Shells," *Journal of Spacecraft and Rockets*, Vol. 6, No. 5, May 1969, pp. 603–609.

[20] Forsberg, K., "Exact Solution for Natural Frequencies of Ring-Stiffened Cylinders," *AIAA/ASME 10th Structures, Structural Dynamics and Materials Conference*, AIAA, New York, 1969.

[21] Egle, D. M. and Soder, K. E., Jr., "A Theoretical Analysis of the Free Vibration of Discretely Stiffened Cylindrical Shells with Arbitrary End Conditions," *AIAA Structural Dynamics and Aeroelasticity Specialist Conference*, AIAA, New York, 1969.